Three-Dimensional Hot-Spot X-Ray Emission Tomography from Cryogenic Deuterium–Tritium Direct-Drive Implosions on OMEGA

K. Churnetski,[1,2] K. M. Woo,[1] W. Theobald,[1,2] P. B. Radha,[1] R. Betti,[1,2,3] V. Gopalaswamy,[1] I. V. Igumenshchev,[1] S. T. Ivancic,[1] M. Michalko,[1] R. C. Shah,[1] C. Stoeckl,[1] C. A. Thomas,[1] and S. P. Regan[1,2]

[1]Laboratory for Laser Energetics, University of Rochester
[2]Department of Mechanical Engineering, University of Rochester
[3]Department of Physics and Astronomy, University of Rochester
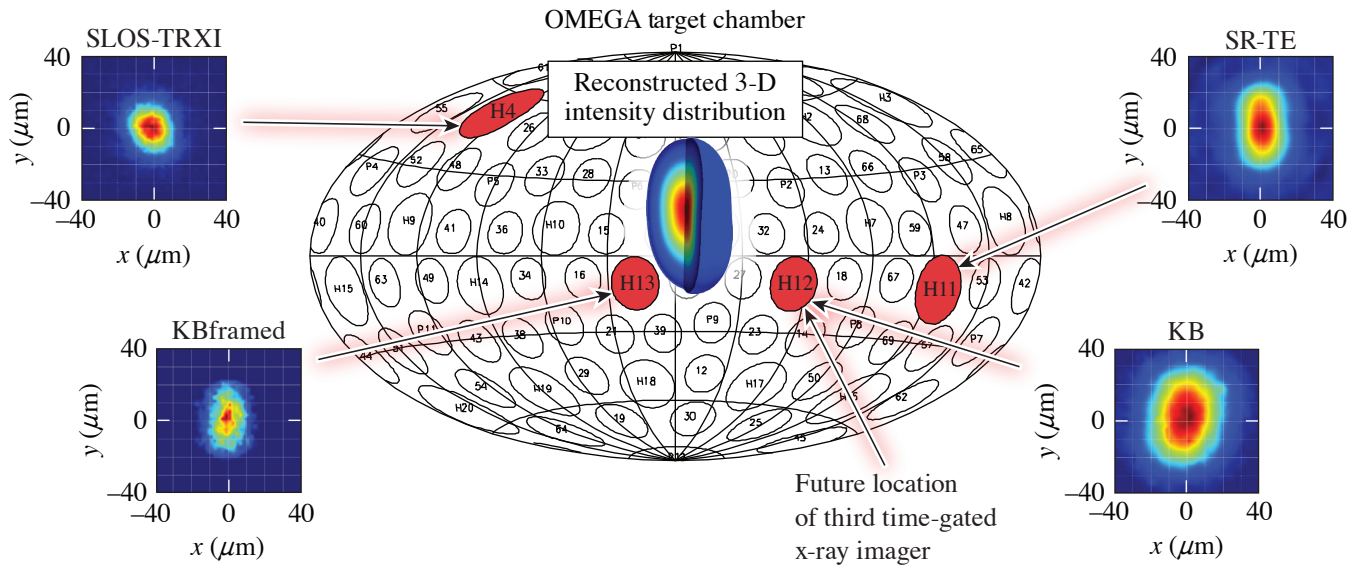
In direct-drive inertial confinement fusion (ICF),[1] laser beams are focused onto a spherical target to implode a thin shell composed of an outer ablation layer (typically plastic) and an inner layer of solid cryogenic deuterium–tritium (DT) fuel. The laser-direct-drive ICF concept is studied on the 60-beam, 30-kJ, 351-nm OMEGA laser,[2] which has produced high-performing implosions with hot-spot pressures exceeding 50 Gbar, described in Ref. 3. The recent application of statistical modeling significantly improved the implosion performance and the neutron yield.[4] Low-mode drive variations in the driver illumination and from target perturbations can significantly impact implosions.[5–7] The goal over the next several years is to further optimize OMEGA implosions and to demonstrate ignition-relevant implosions that when scaled to 2 MJ of laser energy, would enter the burning-plasma regime.[8,9] Three-dimensional hot-spot x-ray emission tomography is a powerful tool to diagnose low-mode asymmetries, which will help to mitigate low-mode perturbations and improve implosion performance. This work is embedded in a long-term project that aims to understand the physics and multidimensional effects that currently limit the hot-spot pressure in ICF implosions on OMEGA and to help to develop strategies to increase the hot-spot pressure.

OMEGA currently has a combination of time-gated and time-integrated x-ray diagnostics for hot-spot imaging along four lines of sight (LOS), which enable a 3-D interpretation of the hot-spot shape. These diagnostics include KBframed,[10] the single line-of-sight, time-resolved x-ray imager (SLOS-TRXI),[11] KB (formerly GMXI),[12] and a spatially resolved electron temperature diagnostic (SR-TE).[13] The diagnostics have different spatial and temporal resolutions, as well as slightly different spectral sensitivities. These four diagnostics are quasi-orthogonal from each other, allowing for a 3-D view of the imploding ICF core. Figure 1 shows the locations of the detectors on the OMEGA target chamber and example data from each detector.

A 3-D hot-spot emission model was developed to reconstruct the hot-spot emission profile of direct-drive implosions on OMEGA by combining the measured x-ray emission data from multiple LOS.[14] The radiation transfer equation along a single LOS is considered for a steady-state plasma in which the temperature and density distributions and the radiation field are independent of time.[15] The hot-spot plasma of cryogenic DT target implosions on OMEGA is optically thin for photon energies >2.5 keV. All of the x-ray imagers considered here satisfy this condition and absorption can be neglected.[13] Neither the absolute signal nor the temporal evolution of the hot-spot emission are taken into account in this simplified model. The spectral response is assumed to be the same for all the x-ray imagers. Using those simplifications and dropping the frequency dependence on the plasma emissivity ε, the projected x-ray image $I_{\hat{s}}$ along an observation direction $\hat{s}$ over a path length s is given by $I_{\hat{s}} \sim \int_{s} \varepsilon \, \mathrm{d}s$.

A method described in Woo et al.[14] has been developed to reconstruct ε through a complete expansion set using both non-orthogonal polynomial and orthogonal polynomial expansions. The complex shape of the hot-spot emission can be described in terms of a model of generalized spherical-harmonic Gaussian functions,

$$\ln \varepsilon(r, \theta, \varphi) = \sum_{n=0}^{\infty} \sigma_n R^n \left[1 + \sum_{\ell=1}^{\infty} \sum_{m=-\ell}^{\ell} \sum_{k=0}^{\infty} A_{\ell m k} R^k Y_{\ell m}(\theta, \varphi) \right]^n. \tag{1}$$

E29904JR

Figure 1

The locations of the existing four hot-spot x-ray imaging detectors on the OMEGA target chamber are indicated by the red circles. SLOS-TRXI is located in port H4 (45°, 234°), KBframed in port H13 (105°, 342°), KB in port H12 (96°, 54°), and SR-TE in port H11 (101°, 134°). The future third time-gated x-ray imager will also be located in port H12 (96°, 54°). Example data are shown for each diagnostic and the reconstructed 3-D hot-spot emission is displayed in the target chamber center. The polar and azimuthal angles for each detector are denoted in parenthesis.

The emissivity is described in spherical coordinates (r, θ, φ), where the origin of the coordinate system coincides with the peak of ε. In Eq. (1), R is the radius and $Y_{\ell,m}$ are the real spherical harmonic functions. The expansion coefficients, φ_n and $A_{\ell,m}$, are determined by a gradient-descent, machine-learning algorithm that minimizes a loss function, which is the fit error between the model and the normalized measured x-ray images.

To reconstruct the emission profile, an initial estimate is made for the solution of of ε, which is a 1-D Gaussian profile. This model is projected into the LOS of the x-ray detectors using a ray-tracing routine and the projections are compared with the experimental x-ray images from each diagnostic. The error between the model and the experimental images is calculated as the sum of the root-mean-square (rms) difference over the multiple lines of sight. The coefficients of the model are slightly perturbed, and this process is repeated for several iterations until the rms error is minimized.

Proof-of-principle simulations with the hydrodynamic code $DEC3D$[16] assuming a mode-2 perturbation were used to validate the 3-D reconstruction procedure. The result of the simulation was post-processed with the detector resolutions and spectral sensitivities using $Spect3D$[17] to create simulated x-ray images along the four lines of sight. Normally distributed random noise was added to the simulated x-ray images, and the hot-spot emission was reconstructed multiple times in a Monte Carlo simulation by varying the noise. The resulting 3-D reconstructions were projected along the detector lines of sight and the major and minor radii were calculated at the 1/e contour level for the reconstruction projections and simulated x-ray images. The radii agreed within the error bars, which gives confidence in the viability of this technique.

A direct-drive ICF campaign on OMEGA was conducted with deliberate laser-drive asymmetries to study the effect of hot-spot shape asymmetries on implosion performance. The polar-direct drive (PDD)[18] beam illumination geometry was applied by using 40 of the 60 OMEGA beams, switching off 20 beams around the equator. The 40 beams are grouped in three beam rings in the upper and lower hemisphere according to their polar angles.[18] The partition of beam energies in rings 1 and 3 was varied while keeping the total laser energy constant. The magnitude of the laser-drive asymmetry was varied to produce hot spots that

ranged from oblate to prolate in shape. Figure 2 shows data from three shots at stagnation from KBframed, which has an equatorial view of the capsule. Reconstructions were done for each shot during this campaign and compared to the experimental inputs.
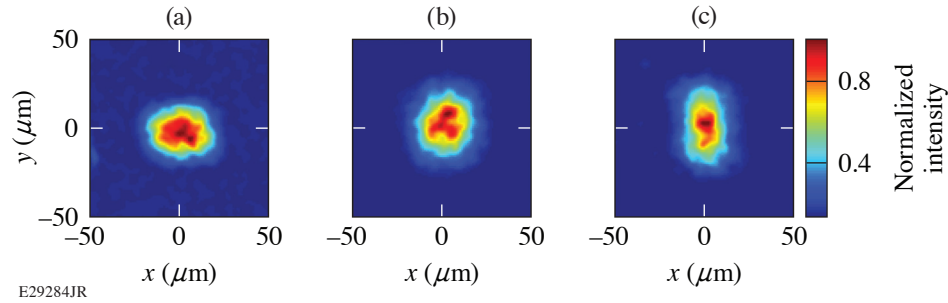

E29284JR

Figure 2

Experimental x-ray images from the KBframed diagnostic at stagnation of cryogenic DT target implosions performed with the PDD illumination geometry. The beam-energy balance was varied from a stronger drive on (a) the poles (shot 96578), to (b) a balanced drive (shot 96575), to (c) a stronger drive on the equator (shot 96581), while keeping the total laser energy conserved.

The reconstruction of shot 96581 is shown in Fig. 1. Data from SLOS-TRXI and KBframed are chosen to be from the time of peak emission, and data from KB channel 3 and SRTE channel 1 are used due to the similar energy ranges to those of SLOS-TRXI and KBframed. The differences in hot-spot size between the different diagnostics can be attributed to differences in time resolution. With a higher intensity of laser energy incident at the equator of the capsule, a prolate shape is expected in the hot-spot emission with the major axis aligned with the z axis of the target chamber. Spherical harmonic modes up to $\ell = 3$ were used in the reconstruction. The large $A_{2,0} = -0.47 \pm 0.03$ expansion coefficient indicates a strong mode $\ell = 2$ in the reconstruction, which can be seen in the experimental x-ray images. The $A_{2,0}$ coefficient is negative, which indicates a prolate shape and is consistent with what we expect from the laser-drive asymmetry. Reconstructions of other shots from this campaign also show the expected overall shape and orientation of the hot spot based on the laser-drive asymmetry and will be further discussed in a future publication.

1. R. S. Craxton *et al.*, Phys. Plasmas **22**, 110501 (2015).
2. T. R. Boehly *et al.*, Opt. Commun. **133**, 495 (1997).
3. S. P. Regan *et al.*, Phys. Rev. Lett. **117**, 025001 (2016); 059903(E) (2016).
4. V. Gopalaswamy *et al.*, Nature **565**, 581 (2019).
5. B. K. Spears *et al.*, Phys. Plasmas **21**, 042702 (2014).
6. O. M. Mannion *et al.*, Phys. Plasmas **28**, 042701 (2021).
7. H. G. Rinderknecht *et al.*, Phys. Rev. Lett. **124**, 145002 (2020).
8. O. A. Hurricane *et al.*, Phys. Plasmas **26**, 052704 (2019).
9. A. B. Zylstra *et al.*, Nature **601**, 542 (2022).
10. F. J. Marshall *et al.*, Rev. Sci. Instrum. **88**, 093702 (2017).)
11. W. Theobald *et al.*, Rev. Sci. Instrum. **89**, 10G117 (2018).
12. F. J. Marshall and J. A. Oertel, Rev. Sci. Instrum. **68**, 735 (1997).
13. D. Cao *et al.*, Phys. Plasmas **26**, 082709 (2019).
14. K. M. Woo *et al.*, Phys. Plasmas **29**, 082705 (2022).
15. Ya. B. Zel'dovich and Yu. P. Raizer, *Physics of Shock Waves and High-Temperature Hydrodynamic Phenomena*, edited by W. D. Hayes and R. F. Probstein (Dover, Mineola, NY, 2002).

16. K. M. Woo *et al.*, Phys. Plasmas **25**, 102710 (2018).

17. J. J. MacFarlane *et al.*, High Energy Density Phys. **3**, 181 (2007).

18. P. B. Radha *et al.*, Phys. Plasmas **19**, 082704 (2012).